The diffracted sound field from the transition region of an axisymmetric body in water*

Li Xue-Gang(黎雪刚)†, Yang Kun-De(杨坤德), and Wang Yong(汪 勇)

College of Marine, Northwestern Polytechnical University, Xi'an 710072, *China*

(Received 18 January 2011; revised manuscript received 1 March 2011)

Understanding the physical features of the diffracted sound field on the surface of an axisymmetric body is important for predicting the self-noise of a sonar mounted on an underwater platform. The diffracted sound field from the transition region of an axisymmetric body was calculated by the geometrical theory of diffraction. The diffraction ray between the source point and the receiving point on the surface of an axisymmetric body was calculated by using the dynamic programming method. Based on the diffracted sound field, a simulation scheme for the noise correlation of the conformal array was presented. It was shown that the normalized pressure of the diffracted sound field from the transition region reduced with the increases of the frequency and the curvature of the ray. The flow noises of two models were compared and a rather optimum fore-body geometric shape was given. Furthermore, it was shown that the correlation of the flow noise in the low frequencies was stronger than that in the high frequencies. And the flow noise received by the acoustic array on the curved surface had a stronger correlation than that on the head plane at the designed center frequency, which is important for sonar system design.

Keywords: diffracted sound field, flow noise, uniform geometric theory of diffraction, correlation

PACS: 43.30.Nb, 43.30.Lz **DOI:** 10.1088/1674-1056/20/7/074301

1. Introduction

With the development of stealth technology, the performance of a sonar mounted on an underwater platform is affected increasingly and prominently by the self-noise of the underwater vehicle. If the self-noise level of the underwater body can reduce by 10 dB, the detection range of the sonar will increase 2–3 times under the same condition. The noise sources include hydrodynamic noise, ambient noise, propeller's noise and mechanical noise. Flow noise as the main part of the hydrodynamic noise dominates at high speed. It covers the radiated noise of a target in far field and limits the performance of the sonar mounted on an underwater platform. The flow noise received by the sonar of an axisymmetric body mainly comes from the transition region.[1,2] Due to the obstruction of the body, the performance of the sonar is mainly affected by the diffracted sound field from the transition region. Thus it is necessary to study the diffracted sound field of the flow noise and to find a way to reduce and suppress it.

Recently, several methods have been developed to calculate the structure near field and the surface sound field. The methods include the boundary element method,[3] the Summerfeld–Watson transformation method[4] and the transmission matrix (T-matrix) method.[5] For the boundary element method, due to the limit of the calculation scale, it's hard to calculate the high-frequency sound field. The calculation process of the Summerfeld–Watson transformation method is very complicated. The T-matrix method is applied for a wider frequency range, but cannot be used to calculate the structure with big length-width ratio. Based on the geometrical optics and the geometric acoustics, Levy and Keller[6] presented the geometrical theory of diffraction (GTD). Kouyoumjian and Pathak[7] developed the GTD and presented the uniform geometrical theory of diffraction (UTD), which is applied widely in engineering practice.[8−11] For instance, Pathak[12] analyzed the electromagnetic field between antennas on a convex surface using the UTD method. The report about the application of the UTD method in acoustic calculation

*Project supported by the National Natural Science Foundational of China (Grant No. 10774119), the Program for New Century Excellent Talents in University of Ministry of Education of China (Grant No. NCET-08-0455), the Natural Science Foundation of Shaanxi Province of China (Grant No. SJ08F07), the Foundation of National Laboratory of Acoustics of China, and the Foundation for Fundamental Research of Northwestern Polytechnical University of China (Grant No. 2007004).

†Corresponding author. E-mail: xuegang608@126.com

© 2011 Chinese Physical Society and IOP Publishing Ltd

is very rare. Rens[13] calculated the diffracted sound field of an engine noise by using the UTD method. Lei[14] studied the acoustic forward scattering by a cylindrical shell. These studies both belong to the acoustic radiation problems in far field. Li[15] studied the power spectrum and the correlation of the flow noise of an axisymmetric body by using a numerical method. However this method was limited by the calculation scale and would take a long time for the iteration process of the flow field and the noise field to converge.

In this paper, a quick way to obtain the sound field on the surface of an axisymmetric body was presented. The ray path between the source point and the field point on the surface of an axisymmetric body was traced by using the dynamic programming method. Based on the UTD method, the diffracted sound field on the head surface of the transition region of an axisymmetric body was calculated. The diffraction sound fields of the models were compared and a better model shape from the viewpoint of self-noise was given. Furthermore, based on the diffracted sound field, the correlations of the flow noise field received by the acoustic conformal array were calculated and analyzed.

2. Calculation method for diffracted sound field

2.1. Geometrical theory of diffraction

The asymptotic surface field due to an infinitesimal surface source is developed by generalizing the asymptotic solutions to canonical problems involving the excitation of perfectly conducting circular cylinder and sphere geometries by the point source.[12] According to the uniform geometrical theory of diffraction,[12,16] the asymptotic solution for the pressure field Q on the surface due to the point source Q' is given by

$$\begin{aligned} &\mathrm{d}p(Q|Q') \\ &= \frac{-\mathrm{j}k\rho cu(s)}{4\pi}\left\{2\left[1-\frac{\mathrm{j}}{kr}\right]V(\xi)\right\}DG(kr)\mathrm{d}s, \end{aligned} \quad (1)$$

where Q' and Q denote the source and the field points, respectively, as shown in Fig. 1, r refers to the length of the surface ray path between the source and the observation points, k refers to the wavenumber of the exterior medium (which is taken to be the free space), ρ and c are the density and the sound speed of the medium, respectively and $u(s)$ is the vibration velocity of the infinitesimal source $\mathrm{d}s$.

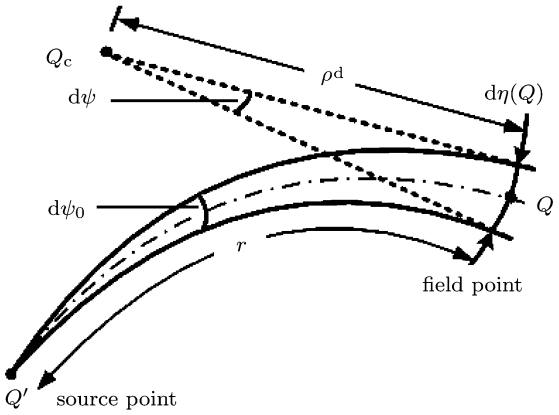


Fig. 1. Surface ray strip.

The function $V(\xi)$ in Eq. (1) is the hard surface Fock integral and is given by

$$V(\xi) = \frac{\xi^{1/2}\,\mathrm{e}^{\mathrm{j}\pi/4}}{2\sqrt{\pi}}\int_{\mathrm{e}^{-\mathrm{j}2\pi/3}}^{\infty}\frac{W_2(\tau)}{W_2'(\tau)}\,\mathrm{e}^{-\mathrm{j}\xi\tau}\,\mathrm{d}\tau, \quad (2)$$

where $W_2(\tau)$ denotes the Fock-type Airy function defined by

$$W_2(\tau) = \frac{1}{\sqrt{\pi}}\int_{\mathrm{e}^{-\mathrm{j}2\pi/3}}^{\infty}\mathrm{e}^{\tau Z - Z^3/3}\mathrm{d}Z, \quad (3)$$

and $W_2'(\tau)$ denotes the derivative of $W_2(\tau)$ with respect to τ. The $V(\xi)$ can be calculated by using the method given in Refs. [16] and [17]. The ξ is the generalized Fock parameter for the arbitrary convex surface and is defined by

$$\xi = \left(\frac{k}{2}\right)^{1/3}\int_{Q'}^{Q}\frac{1}{[\rho_{\mathrm{g}}(r)]^{2/3}}\mathrm{d}r, \quad (4)$$

which is the arc length normalized by the wavenumber k and the radius of the curvature $\rho_{\mathrm{g}}(r)$. Note that $\xi = 0$ defines the lit region, $\xi < 1$ defines the penumbra region and $\xi \gg 1$ defines the deep shadow. Our solution is valid for all $\xi \geq 0$. The $G(kr)$ in Eq. (1) is the Green function in the free field and is given by

$$G(kr) = \frac{\mathrm{e}^{-\mathrm{j}kr}}{r}. \quad (5)$$

The surface ray divergence factor D is given by

$$D = \sqrt{\frac{r\,\mathrm{d}\psi_0}{\mathrm{d}\eta(Q)}} = \sqrt{\frac{r\,\mathrm{d}\psi_0}{\rho^{\mathrm{d}}\,\mathrm{d}\psi}}. \quad (6)$$

In Fig. 1, a pair of infinitesimally separated surface rays adjacent to the central ray from Q to Q' are shown. These adjacent rays constitute a surface strip

and the $\mathrm{d}\psi_0$ in Eq. (5) refers to the angle between these adjacent surface rays at the source point Q'. The $\mathrm{d}\psi$ is the angle between the backward tangents of the same pair of adjacent surface rays at the point Q. The tangents cross at point Q_c. The ρ^d is the distance between points Q and Q_c. The $\mathrm{d}\eta(Q)$ denotes the width of the surface ray strip at the point Q. According to the generalized Fermat's principle, rays are shed or diffracted from the surface ray along the forward tangents of the geodesic surface ray path. Hence, energy is continuously lost from the surface ray field due to rays shed or diffracted from the surface ray.

The asymptotic solution for the pressure field can be calculated by adding the entire infinitesimal sources on the surface. Assuming that S is the vibration area on the surface, the total pressure in the field point Q caused by the vibration area S can be written as

$$\bar{p}(Q|S) = \int_S \frac{-\mathrm{j}k\rho cu(s)}{4\pi}\left\{2\left[1-\frac{\mathrm{j}}{kr}\right]V(\xi)\right\}DG(kr)\mathrm{d}s. \quad (7)$$

2.2. Surface ray tracing

The simplified model and the boundary layer of an axisymmetric body are show in Figs. 2(a) and 2(b), respectively. The source of flow noise under consideration locates at the transition region and the turbulent boundary layer on the axisymmetric body. Lauchle[1] has shown that the noise measured in the laminar region (including the stagnation point)

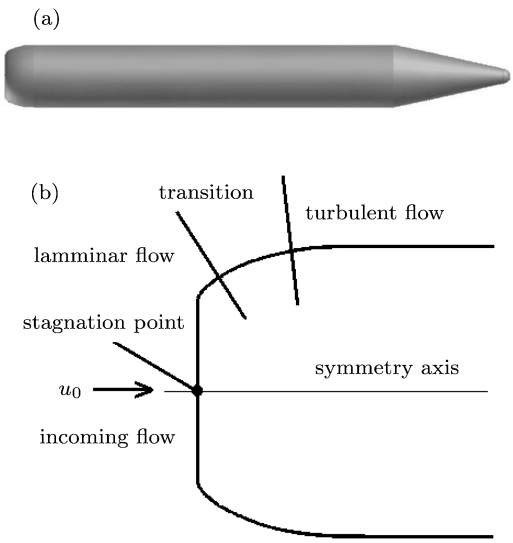


Fig. 2. The axisymmetric body: (a) the simplified model and (b) the boundary layer.

corresponds closely to the noise measured in the transition region, provided that the acoustic losses due to the diffraction have been accounted for. Experiment results[2] show that when the frequency of the flow noise is less than 40 kHz, the flow noise received at the stagnation point of the axisymmetric body mainly comes from the transition region.

In order to calculate the diffracted sound field, the surface ray should be traced exactly. The flow noise from the transition region is assumed to be the dominant source and is considered as a ring of uncorrelated point sources. The 60 discrete point sources are set uniformity at the transition region to simulate the source of the flow noise. The position of the transition region can be determined by the method given in Refs. [15] and [18]. As shown in Fig. 3, the transition points are in the plane $z = -a$, where a is the vertical distance from the transition point to the head plane of the axisymmetric body. The position of the point source can be expressed as $(r_0\cos\theta, r_0\sin\theta, -a)$, where r_0 and θ is the radius and the azimuth angle in the transition plane, respectively. A line array with 8 hydrophones is put on the head of the axisymmetric body. The serial numbers of the hydrophones in Fig. 3 are 1#, 2#, ..., 8# from right to left, respectively.

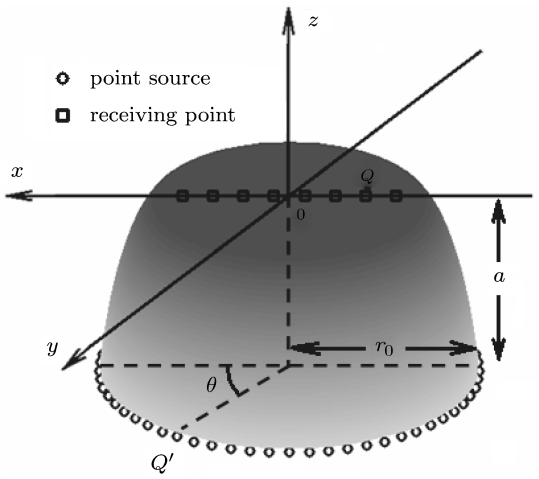


Fig. 3. The head surface of an axisymmetric body.

In the asymptotic high frequency approximation, the source point Q' propagates a distance r along a surface ray path as shown in Fig. 1. The surface ray path satisfies the generalized Fermat's principle proposed by Keller.[19] The Fermat's principle denotes that the surface ray path between the source point Q' and the field point Q on a convex surface is the curve by taking extreme value to the changes of the small sound path. According to the uniform geometrical theory of diffraction, the acoustic pressure in the

field point Q is mainly determined by the surface ray between the source point Q' and the field point Q. In a certain position, there will be high-order diffraction rays between Q' and Q. As the diffraction loss of the high-order ray is very large, we just need to consider the first-order diffraction ray.

According to the Fermat's principle, a dynamic programming method is introduced for ray tracing on any convex surface. As shown in Fig. 4, $p_{\rm s}(u_{\rm s},\, v_{\rm s})$ and $p_{\rm r}(u_{\rm r},\, v_{\rm r})$ are the source and the field points on the convex surface $S(u, v)$, respectively. The region $[v_{\rm s},\, v_{\rm r}]$ is divided into N portions along the boundary line $u = u_{\rm s}$. Then, the $N-1$ coordinate lines of u are determined by the N-1 dividing points. Similarly, the region $[u_{\rm s},\, u_{\rm r}]$ is divided into M portions along the boundary line $v = v_{\rm s}$ and we obtain $M-1$ coordinate lines of v. These u coordinate lines intersect with the v coordinate lines at points p_{ij}, which represent the surface $s(u, v)$ discretely. Obviously, the ray tracing process can be divided into M steps by the $M-1$ v coordinate lines. The stage variable of each step is K ($K = 1,\, 2,\, \ldots,\, M$).

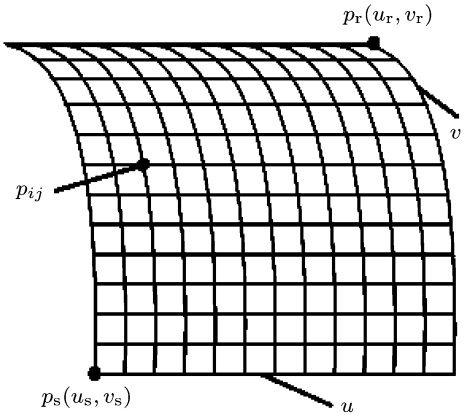


Fig. 4. Surface grid and coordinates

In the first step, the allowed state is $S_1 = \{p_{\rm s}\}$. And in the K step, the optional coordinate nodes are $S_k = \{p_{ij}(u_i, v_j)\}$, where $i < K-1$ and $j = 1,\, 2,\, 3,\, \ldots,\, N$. According to the above segmentation and the variables defined, the iterative process for the ray tracing is given by

$$f_{n+1}(s_{n+1}) = 0, \tag{8}$$

$$f_k(s_k) = \min_{x_k \in D_k} \{d(s_k, x_k) + f_{k+1}(s_{k+1})\}, \tag{9}$$

where $k = n, n-1, \ldots, 1$, $d(s_k,\, x_k) = n_k|s_k x_k|$, n_k is the refractive index of the medium and $|s_k x_k|$ is the distance between s_k and x_k.

The process for the ray tracing follows the following four steps:

(1) For a given convex surface, we should discrete the surface and calculate the coordinate value p_{ij} first.

(2) Assuming $k = n+1$, then $f_k(s_k) = 0$.

(3) Assuming $k = k-1$, $f_k(s_k)$ can be calculated by using Eq. (9), meanwhile x_k is determined, here $s_k \in \{p_{kj},\, j = 1,\, 2,\, \ldots,\, m\}$.

(4) Repeat the step (3) until $k = 1$, then $f_1(s_1)$ is the arc length of the ray traced on the surface. Meanwhile the coordinate nodes crossed by the surface ray can be determined reversely.

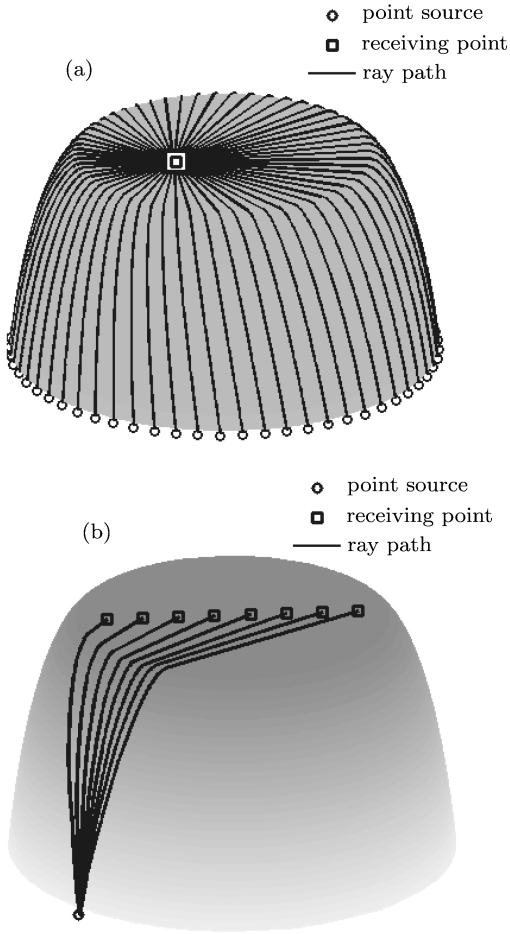


Fig. 5. The ray paths (a) from 60 source points to one receiving point and (b) from 1 source point to 8 receiving points.

As shown in Fig. 2(b), the incoming flow is assumed to be 42 knots (about 21.6 m/s). The position of the transition point can be determined by the method given in Ref. [15]. According to the above recursion algorithm, the surface ray paths on the head of the axisymmetric body are shown in Fig. 5. It is shown in Fig. 5(a) that 60 point sources are laid in a circle, which is 85 mm away from the head plane of

the axisymmetric body and the radius of the circle r_0 is 155 mm. The coordinate of the receiving point is (37.5 mm, 0, 0). In Fig. 5(b), the position of the point source θ is 42°. A line array with 8 receiving points is laid on the head of the axisymmetric body and the distance of the adjacent elements is 25 mm. It can be seen that the ray path between the source point and the receiving point on the surface of the axisymmetric body is calculated accurately by the method of dynamic programming.

2.3. Calculation of the correlation

The correlation of the noise received by the acoustic array is important to improve the performance of a sonar mounted on an underwater platform. The correlation of the flow noise from the transition region of an axisymmetric body is simulated in this section. As shown in Fig. 3, a line array with 8 hydrophones is laid on the head of the axisymmetric body. First, 60 independent narrowband Gaussian noise sequences n_k ($k = 1, 2, \ldots, 60$) are created by the numerical method and the center frequency is assumed to be 30 kHz. The mean value and the variance of the sequences are 0 and δ, respectively. Assuming that the phase difference and the amplitude variation from the source point k to the i-th hydrophone are ϕ_{ki} and A_{ki}, respectively, then the noise sequence received in the i-th hydrophone can be written as

$$x_i = \sum_{k=1}^{60} n_k \cdot A_{ki}\, \mathrm{e}^{-\mathrm{j}\phi_{ki}}. \tag{10}$$

For any two hydrophones i and j, the correlation coefficient of the flow noise is given by

$$\rho_{ij} = \frac{E(x_i x_j^*)}{\sqrt{\mathrm{var}\,(x_i) \cdot \mathrm{var}\,(x_j)}}, \tag{11}$$

where E and the superscript $*$ denote the mean value and the conjugate, respectively and var means variance.

2.4. Calculation process of the flow noise

The calculation process of the flow noise for an axisymmetric body is shown in Fig. 6. When the geometric shape of an axisymmetric body is given, the boundary layer transition region can be calculated by the method given in Li's paper.[15] As the flow noise at the head of the axisymmetric body mainly comes from the transition region, discrete points sources are set uniformity at the transition region to simulate the source of the flow noise. The flow noise field can be calculated by using the UTD method. Then the diffracted pressure at the receiving points and the noise correlation can be calculated. Through the study of the sound pressure level of the flow noise, we can optimize and design the fore-body shape of an axisymmetric body to reduce the noise. Meanwhile we can try to make full use of the noise correlation in the acoustic array signal processing, which will be our future work.

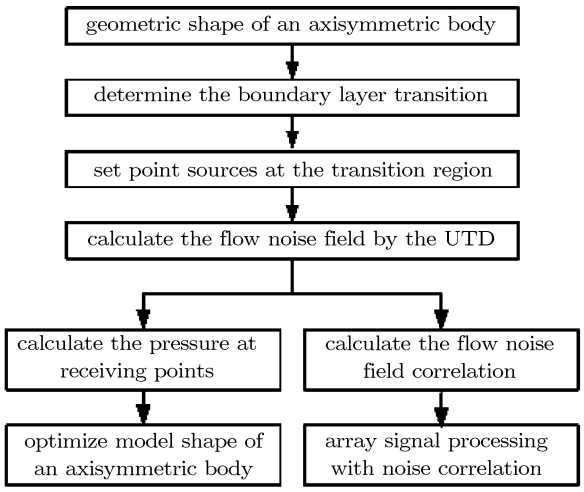


Fig. 6. The calculation process of the flow noise.

3. Solution for the diffraction sound field

3.1. The features of the diffraction sound field

Based on the sound ray path given in Section 2.2, the normalized sound pressures along the z coordinates of the surface ray can be calculated by using the uniform geometrical theory of diffraction given in Eq. (7). The frequency is assumed to be 30 kHz. In Fig. 7(a), the dotted and the solid lines denote the diffraction losses of the ray paths from positions $\theta = 6°$ and $\theta = 6°$ to 2# hydrophone, respectively. It is shown that the normalized pressures decline rapidly at the beginning of both rays and then slowdown. In addition, the diffraction loss of the ray from position $\theta = 96°$ is larger than that of the ray from position $\theta = 6°$ at the beginning of the rays. That is because the ray curvature of the ray from position $\theta = 96°$ is larger than that of the ray from position $\theta = 6°$ at the beginning of the rays. Due to the changes of the ray curvature on the surface, the diffraction losses of

both rays increase significantly faster close to the head plane ($z = 0$ plane) of the axisymmetric body and the diffraction loss of the ray from position $\theta = 6°$ become larger than that of the ray from position $\theta = 96°$. In Fig. 7(b), the dotted and the solid lines denote the ray paths from the source point in the position $\theta = 90°$ to 1# and 4# hydrophones, respectively. It can be seen that the conclusions are similar to that of Fig. 7(a). So the diffraction loss becomes larger with the increase of the ray curvature.

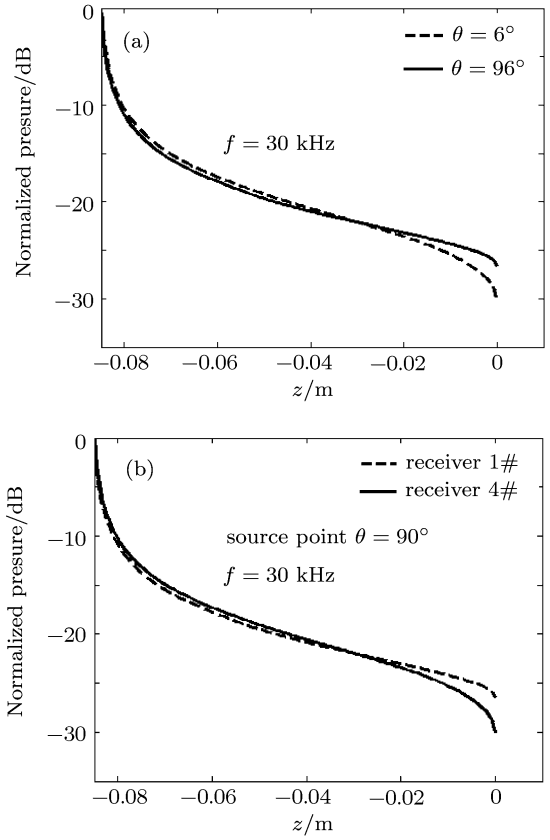


Fig. 7. Diffraction losses (a) form different sources and (b) at different hydrophones.

The normalized pressures recorded at 1#, 2#, 3# and 4# hydrophones are shown in Figs. 8(a), 8(b), 8(c) and 8(d), respectively. It can be seen from Fig. 8(a) that the variation of the pressure with position θ at 1# hydrophone is larger than that at other hydrophones and the maximum value is about 4 dB larger than the minimum one. The reason is that the acoustic paths and the curvatures of the rays from different positions have larger difference for the 1# hydrophone. On the contrary, as shown in Fig. 8(d), since the 4# hydrophone is close to the stagnation point of the axisymmetric body, the acoustic paths and the curvatures of the rays from different positions have smaller difference. The difference between the maximum and the minimum values is small and is about 0.1 dB, which is far less than that of the 1# hydrophone.

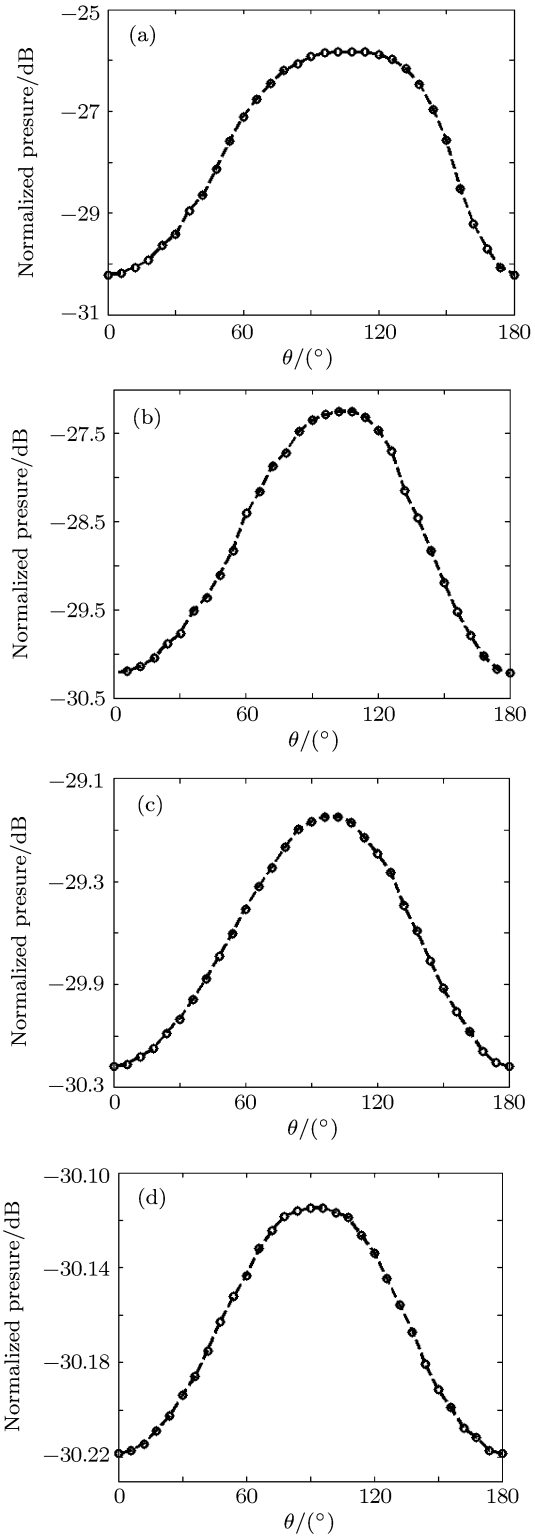


Fig. 8. The normalized pressure at (a) 1#, (b) 2#, (c) 3# and (d) 4# hydrophones.

3.2. Optimization of an axisymmetric body

Based on the above method, the pressures of two models with different fore-body shapes are calculated. As shown in Fig. 9(a), the diameter of model A is larger than that of model B at the head of the axisymmetric body. In other parts, the geometries of the two models are identical. The fluid velocity is assumed to be 42 knots (about 21.6 m/s). The transition points are 85 mm and 115 mm away from the peak plane for model A and model B, respectively. It can be seen that the transition points of the two models have a large difference, though the shapes of the two models have a small difference. The diffraction losses of the ray paths from source point $\theta = 0°$ to the stagnation point for model A and model B are shown in Fig. 9(b). It is shown that the normalized pressure of model A in the stagnation point is about 2 dB larger than that of model B. Figure 9(c) shows the diffraction losses received at the stagnation points changing with the frequency for the two models. It is seen that the diffraction losses at the stagnation points increase with the frequency. The normalized pressure of model A is about 2 dB larger than that of model B from 10 kHz to 40 kHz, which means the self-noise level of model B is about 2 dB smaller than that of model A when the source level is the same. So the fore-body shape of model B is better than that of model A, which could be used to design an axisymmetric body with smaller self-noise.

The surface sound fields of the two models are shown in Fig. 10. The frequency is assumed to be 30 kHz. It can be seen that the sound radiation from the transition region attenuates rapidly near the transition region but decreases slowly near the stagnation point. And the normalized pressure of model A is higher than that of model B at the same position.

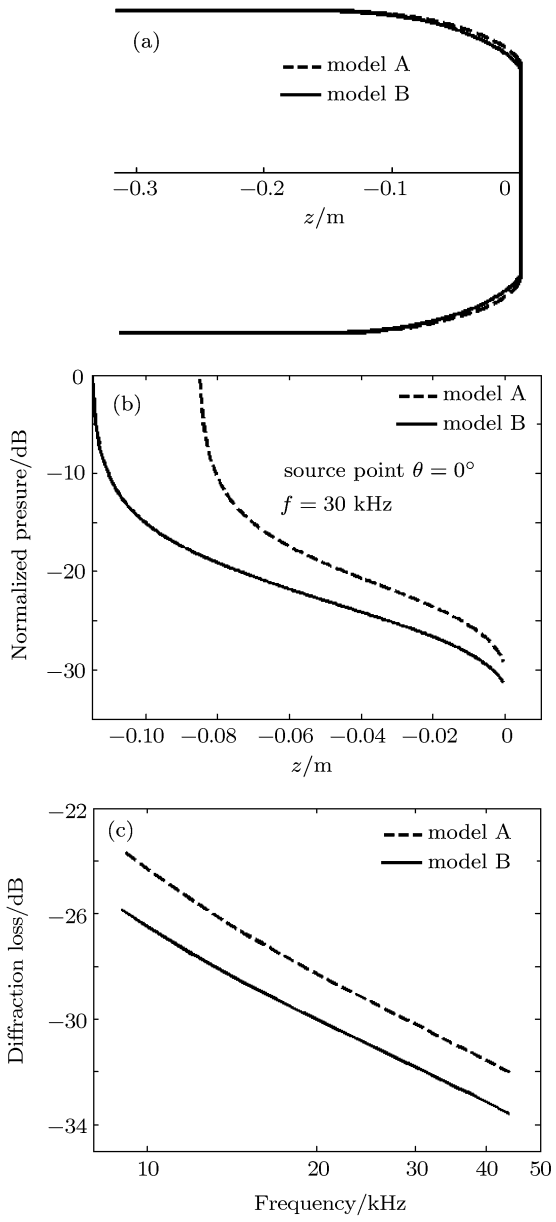


Fig. 9. (a) Two models with different fore-body shapes. (b) Diffraction loss of the ray path. (c) Diffraction loss changing with the frequency.

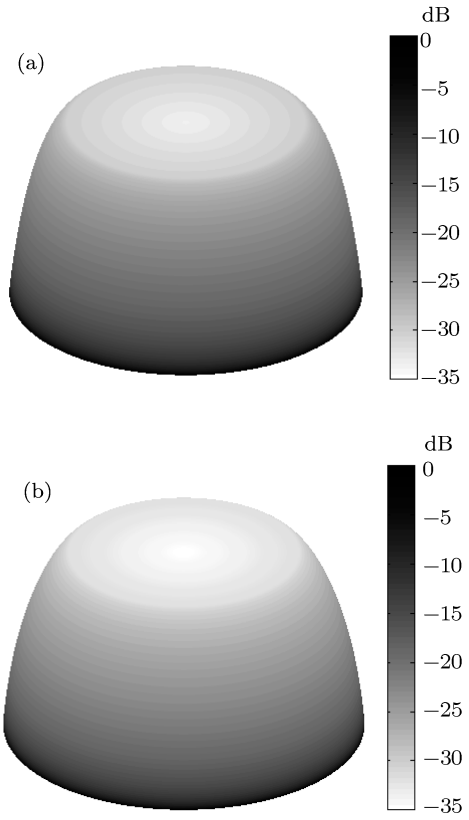


Fig. 10. The surface sound field of (a) model A and (b) model B.

3.3. Correlation of the flow noise

The correlations of the flow noise received at the hydrophones are shown in Fig. 11. The distance between the adjacent hydrophones is 25 mm. The designed center frequency is 30 kHz based on the array configuration method of half-wavelength. The grey scale of each square denotes the correlation coefficient of the two hydrophones corresponding to the square. The bandwidths of the flow noise in Figs. 11(a) and 11(b) are 0.5 kHz and 1 kHz, respectively. It is shown that the flow noise received at the hydrophones has lower correlation and has no obvious features at the designed center frequency, which are important for the sonar system design.

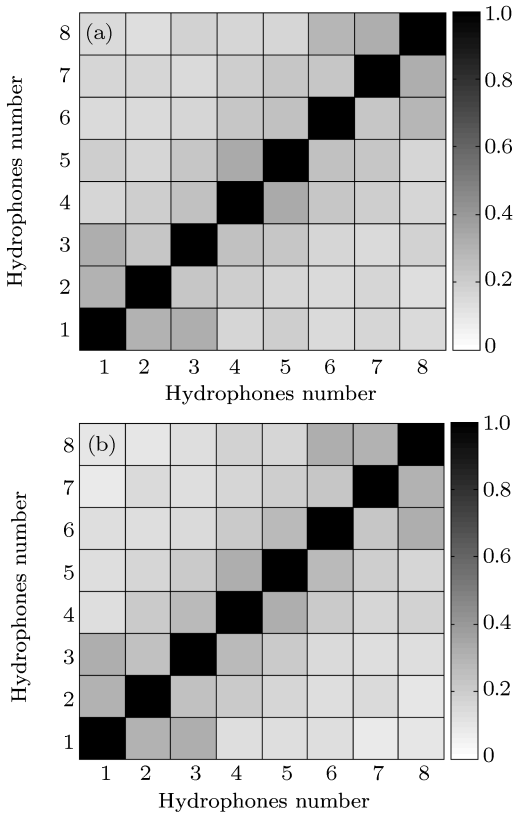


Fig. 11. The correlation of hydrophones with the bandwidths of (a) 0.5 kHz and (b) 1 kHz.

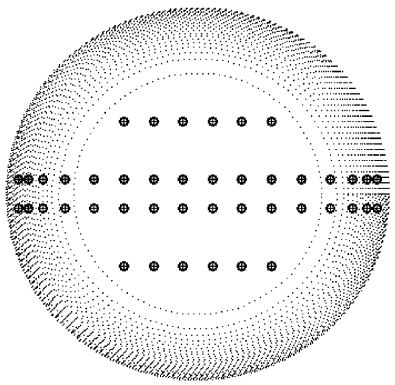


Fig. 12. The simplified model of the conformal array.

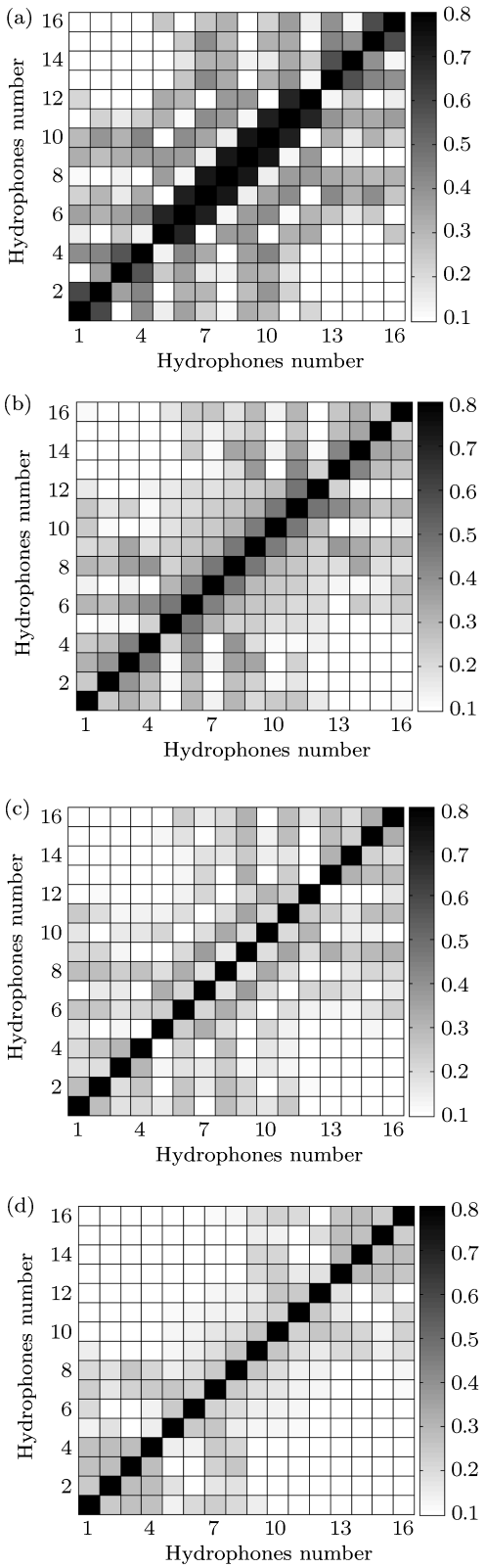


Fig. 13. The correlation of hydrophones in the second line with center frequency at (a) 10 kHz, (b) 15 kHz, (c) 20 kHz and (d) 30 kHz.

The correlation of the flow noise received by the conformal array is also calculated. The simplified model of the conformal array is shown in Fig. 12. The

distance between the adjacent hydrophones is 25 mm. The designed center frequency is 30 kHz based on the array configuration method of half-wavelength. The serial numbers of the hydrophones at the second line are 1#, 2#, ..., 16# from left to right, respectively.

The correlations of the 16 hydrophones at the second line in Fig. 12 are show in Fig. 13. The center frequencies of the flow noise in Figs. 12(a), 12(b), 12(c) and 12(d) are 10 kHz, 15 kHz, 20 kHz and 30 kHz, respectively. The bandwidth of the flow noise is 1 kHz. The range of the grey scale in Fig. 12 is set at 0.1–0.8 to show the correlation clearly. The autocorrelation coefficient at the secondary diagonal is 1.0 in Fig. 13. It can be seen that the correlations in the low frequencies are stronger than that in the high frequencies. Because these frequencies are lower than the designed center frequency. It can also be seen that the correlations of the hydrophones on the curved surface are stronger than that on the head plane at the designed center frequency. The reason is that the flow noises to the hydrophones on the curved surface mainly come from the point sources that are close to these hydrophones. And the flow noises of the hydrophones on the head plane come from all point sources.

4. Conclusions

Understanding the physical features of the flow noise for an axisymmetric body is important, as it can improve the performance of a sonar mounted on an underwater platform. The diffracted sound field on the head surface of an axisymmetric body was calculated by using the uniform geometrical theory of diffraction. Based on the diffracted sound field, the correlation of the noise received by the hydrophones mounted on the axisymmetric body was presented. The correlations of the flow noise field for arbitrary arrays can be calculated in this method. The following results were obtained. (i) The ray path between the source point and the receiving point on the surface of the axisymmetric body was accurately calculated by using the dynamic programming method. The sound radiation from the transition region reduced with the increase of the frequency and the curvature. (ii) By comparing the flow noise of the two models, a rather optimum fore-body shape was given, which could be used to design an axisymmetric body with minimum self-noise. (iii) The correlation of the flow noise in the low frequencies was stronger than that in the high frequencies. And the flow noise received by the acoustic array on the curved surface had stronger correlation than that on the head plane at the designed center frequency, which is important for sonar system design.

The experiment designed to confirm the physical features of the flow noise, such as the diffracted sound field and the correlations, will be the future work. Meanwhile, it is also valuable to make full use of the noise correlation in the acoustic array signal processing.

References

[1] Lauchle G C 1980 *J. Acoust. Soc. Am.* **67** 158

[2] Arakeri V H, Satyanarayan S G, Mani K and Sharma S D 1991 *J. Sound. Vib.* **146** 449

[3] Schenck H A 1968 *J. Acoust. Soc. Am.* **44** 41

[4] Rummerman M L 1992 *J. Acoust. Soc. Am.* **91** 2502

[5] Gaunaurd G C and Werby W F 1990 *Appl. Mech. Rev.* **43** 171

[6] Levy B and Keller J B 1959 *Commun. Pure. Appl. Math.* **12** 159

[7] Kouyoumjian R G and Pathak P H 1974 *Pro. IEEE.* **62** 1448

[8] Rousseau P R and Pathak P H 1995 *IEEE Trans. Antennas Propagat.* **43** 1375

[9] Holm P D 1996 *IEEE Trans. Antennas Propagat.* **44** 879

[10] Volakis J 1986 *IEEE Trans. Antennas Propagat.* **34** 172

[11] Veruttipong T W 1990 *IEEE Trans. Antennas Propagat.* **38** 1757

[12] Pathak P H and Wang N 1981 *IEEE Trans. Antennas Propagat.* **29** 911

[13] Rens J R P, Rens B J E, Holten T and Ruijgrok G J J 2000 AIAA **A00-31088** 1

[14] Lei B, Yang K D and Ma Y L 2010 *Chin. Phys.* B **19** 054301

[15] Li X G, Yang K D and Wang Y 2011 *Chin. Phys.* B **20** 101781

[16] Wang M G 1994 *Geometrical Theory of diffraction* (Xi'an: Xidian University Press) p. 260 (in Chinese)

[17] Lee S W 1978 *IEEE Trans. Antennas Propagat.* **26** 593

[18] Huang J Q and Zhang Y W 1989 *Hydromechanics of an Axisymmetric Body* (Xi'an: Northwestern Polytechnical University Press) p. 112 (in Chinese)

[19] Keller J B 1962 *J. Opt. Soc. Am.* **52** 116